Geomorphology 273 (2016) 217–235

Contents lists available at ScienceDirect

Geomorphology

journal homepage: www.elsevier.com/locate/geomorph

Quantitative risk assessment of landslides triggered by earthquakes and rainfall based on direct costs of urban buildings

Johnny Alexander Vega, Cesar Augusto Hidalgo *

School of Engineering, Civil Engineering Program at University of Medellin, Medellin, Colombia

ARTICLE INFO

Article history:
Received 8 July 2015
Received in revised form 29 June 2016
Accepted 21 July 2016
Available online 26 July 2016

Keywords:
Earthquake
GIS
Hazard
Landslide
Risk
Vulnerability

ABSTRACT

This paper outlines a framework for risk assessment of landslides triggered by earthquakes and rainfall in urban buildings in the city of Medellín - Colombia, applying a model that uses a geographic information system (GIS). We applied a computer model that includes topographic, geological, geotechnical and hydrological features of the study area to assess landslide hazards using the Newmark's pseudo-static method, together with a probabilistic approach based on the first order and second moment method (FOSM). The physical vulnerability assessment of buildings was conducted using structural fragility indexes, as well as the definition of damage level of buildings via decision trees and using Medellin's cadastral inventory data. The probability of occurrence of a landslide was calculated assuming that an earthquake produces horizontal ground acceleration (A_h) and considering the uncertainty of the geotechnical parameters and the soil saturation conditions of the ground. The probability of occurrence was multiplied by the structural fragility index values and by the replacement value of structures. The model implemented aims to quantify the risk caused by this kind of disaster in an area of the city of Medellín based on different values of A_h and an analysis of the damage costs of this disaster to buildings under different scenarios and structural conditions. Currently, 62% of "Valle de Aburra" where the study area is located is under very low condition of landslide hazard and 38% is under low condition. If all buildings in the study area fulfilled the requirements of the Colombian building code, the costs of a landslide would be reduced 63% compared with the current condition. An earthquake with a return period of 475 years was used in this analysis according to the seismic microzonation study in 2002.

1. Introduction

In mountain regions, landslides and slope stability are important issues in urban planning. Occasionally urban residential areas coincide with mountainous terrain, which means that the risk is higher for people in those areas. When there is a landslide disaster, economic costs include relocating communities, repairing physical structures and restoring water quality in streams and rivers (Dragicevic et al., 2015). In many developing countries, where there is a disorderly occupation of land, some of the large cities grow in landslide-prone areas due to its geographical, geological and geomorphological conditions. Therefore, in those areas people live under the threat of natural disaster (Saboya et al., 2006).

Landslides in mountain regions have been studied in relation to physical (e.g. Remondo et al., 2008; Jaiswal and Van Westen, 2009; Jaiswal et al., 2010; Borgomeo et al., 2014) and economic features (e.g. Zêrere et al., 2008; Campos et al., 2012; Vega, 2013). Studies on landslide risk analysis, however, generally evaluate only susceptibility and do not consider vulnerability. Furthermore, landslide hazards are usually estimated from map algebra and historical data without considering the behavior of geo-materials and failure mechanisms (e.g. Mancini et al., 2010; Epifânio et al., 2014; Faraji Sabokbar et al., 2014). In the case of hazard and vulnerability assessments, the municipal cadastral records have been widely applied (e.g. Botero, 2009; Panahi et al., 2011; Vega, 2013), and in general, hazard, vulnerability and risk assessments, they all use GIS (geographic information systems) (e.g. Van Westen et al., 2008; Van Westen, 2013, Martha et al., 2013; Promper et al., 2014; Torkashvand et al., 2014).

Colombia is located in the northwestern corner of South America and has an area of 1,141,748 km^2. About 35% of people in this country live in the Andean region. The Andes are made up of a complex mountain range that crosses the country from North to South and are subject to significant seismic activity. Located in the humid tropics, the country is influenced by the Intertropical Convergence Zone that generates abundant precipitation with bimodal distribution in the Andes, which means two wet periods per year (i.e. March–May and September–November). In Colombia, natural disasters have caused a loss of approximately US$ 7.1 billion in the last 40 years, i.e. an average annual loss of US$177 million. From 1970 to 2011, over 28,000 disastrous events were reported. Between 2000 and 2009, the frequency of this type of events was higher (around 9270 events) compared to the period between

* Corresponding author.
E-mail addresses: javega@udem.edu.co (J.A. Vega), chidalgo@udem.edu.co (C.A. Hidalgo).

http://dx.doi.org/10.1016/j.geomorph.2016.07.032
0169-555X/

1970 and 1979 (around 5657 events). This is associated with both the availability of relevant information sources and the increased population and assets (Campos et al., 2012). In the last 40 years, >1 million homes have been affected by natural disasters including floods (73%), earthquakes (7%) and landslides (5%). 190,000 homes were destroyed between 1970 and 2011, of which about 9% were landslide-related (Campos et al., 2012).

Landslides are triggered by several factors such as earthquakes and rainfall, and constitute one of the principal causes of disasters in the world (Hidalgo, 2013). In Colombia, landslides and floods are natural phenomena that generate the highest impact and risk levels, threatening the social and economic development of the country (Vega, 2013).

Due to different social and economic causes, the city of Medellin has grown rapidly with unplanned occupation of the area, resulting in inadequate urbanization on hillsides with vulnerable buildings and infrastructures. This city is located in the valley called "Valle de Aburrá" (VA), where landslides have caused considerable economic and human losses. In VA, 35% of damages to buildings and 74% of deaths caused by natural disasters are landslide-related (Aristizábal et al., 2010). This differs significantly from the global average; only 14% of economic losses and 0.53% of deaths from natural disasters are attributed to landslides (Bonachea, 2006; Chowdhury et al., 2010).

In this paper, we propose an approach based on physical and probabilistic models to estimate the risk of landslides as an application suitable for urban areas in mountainous regions. The northeastern side of the city of Medellin was used as a case study.

2. Methodology

Risk is defined as the number of casualties, injuries, property damage and effects on economic activities resulting from the occurrence of a disastrous event known as hazard, and its effect on exposed elements according to their level of vulnerability (Vega, 2013). The following equation is used to calculate landslide risks:

$$R = P[T] \times P[C|T] \times u(C) \tag{1}$$

where R is the risk and $P[T]$ is the hazard which in this case is the probability of occurrence of a landslide. $P[C|T]$ is vulnerability as the conditional probability of damage considering that a failure has already occurred and $u(C)$ is the cost of the consequences. Although failures may be caused only by gravity, they are usually triggered by earthquakes or rainfall. A model was developed for hazard evaluation (Fig. 1) in order to calculate the probability of failure using a reliability index. The model first estimates the probability that the factor of safety (FOS) less than unity using the reliability index β, and then it calculates the probability that the acceleration generated by an earthquake (A_h) exceeds a parameter called critical acceleration (A_c), i.e. $P[T] = P(A_h > A_c)$ using the modified reliability index θ.

$$\beta = \frac{E[FOS] - 1}{\sigma[FOS]} \tag{2}$$

$$\theta = \frac{E[Ac] - A_h}{\sigma_{A_c}} \tag{3}$$

In Eq. (2), $E[FOS]$ is the deterministic FOS value calculated from the mean values of the independent variables, and $\sigma[FOS]$ is the standard deviation of FOS (Christian et al., 1994). In Eq. (3), $E[A_c]$ is the expected value of the critical acceleration, A_h is the acceleration of the design earthquake or the most probable earthquake in the study area for a period of return, and σA_c is the standard deviation of the critical acceleration.

It should be noted that Eqs. (2) and (3) are only valid if the probability distribution function (PDF) of FOS is normal; otherwise other formulas should be used (Christian et al., 1994; Baecher and Christian, 2003). In this work normal PDF is assumed for all variables.

Critical acceleration is calculated taking into account the effect of earthquakes using Newmark's method (Newmark, 1965), based on a model of infinite slope stability. According to this method, A_c is a reliable criterion to assess slope stability (Chen et al., 2014). In order to do that, a pseudo-static method is used. In this method, the force of an earthquake is added to the model as a fraction of the weight of the sliding mass. This

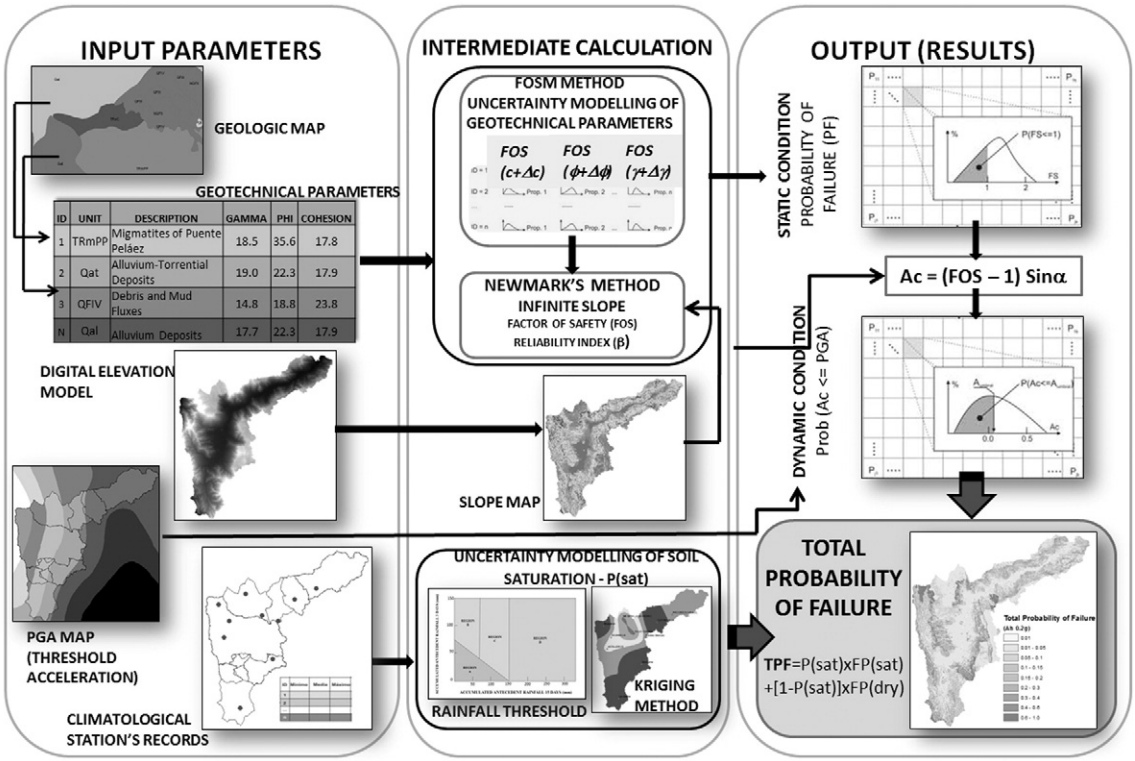

Fig. 1. Schematic methodology adopted for hazard assessment.

Table 1
Classification of hazardous areas according to the annual probability of failure (Chowdhury et al., 2010).

Category	Annual Probability of Failure
Very High	>0.2
High	0.02 – 0.2
Middle	0.002 – 0.02
Low	0.0002 – 0.002
Very low	<0.0002

method is useful for evaluating the stability of shallow slides. The resulting expression for the infinite slope model that we will use in this work is:

$$A_c = (FOS-1)\sin\alpha \tag{4}$$

where α is the average slope angle (°) and *FOS* is calculated as:

$$FOS = \frac{c}{\gamma H(\sin\alpha + A_h\cos\alpha)} + \frac{(\gamma H - \gamma_w H_w)\cos\alpha\tan\varphi}{\gamma H(\sin\alpha + A_h\cos\alpha)} \tag{5}$$

where A_h is given in terms of acceleration caused by gravity g (m s^{-2}), H is the thickness of the failure zone (m), H_w is the water height measured from the failure surface (m), c is soil cohesion (kPa), φ is the angle of internal friction of the soil (°), γ is the unit weight of soil (kN m^{-3}) and γ_w is the unit weight of water (kN m^{-3}).

Landslides most often occur in rainy seasons when there is increased soil saturation with a consequent drop in its cohesion and an increase in pore pressure. The process of decreasing the shear strength caused by changes in the water content is highly complex and it was not considered in the development of this study. Therefore, saturation effect only takes into account an increase of water pressure. Moreover, in this study two situations were considered for H_w: the first one was the presence of the water level in the most critical condition, i.e. $H_w = H$, and the second one was the most favorable condition ($H_w = 0$). Although landslides triggered by rainfall tend to be very shallow, in this research the evaluation was done for a failure surface with a depth of 5 m as the combined effects of rainfall and seismic action are considered to generate deeper failure surfaces. In previous studies, surfaces with depths of 2 and 3 m have been evaluated (Vega, 2013).

Once the critical acceleration that sets the boundary condition on a slope is determined, it is possible to estimate the slope displacement due to a seismic event. That movement is known as Newmark's displacement (*ND*) and regression equations are used for model-based calculations with a parameter of ground motion such as Arias Intensity:

$$\log ND = 1.521\log Ia - 1.993\log A_c - 1.546 \tag{6}$$

$$Ia = 0.9T(PGA)^2 \tag{7}$$

$$\log T = 0.432M - 1.830 \tag{8}$$

where *ND* is Newmark's displacement (cm), *Ia* is Arias intensity (m s^{-1}), *T* is the Dobry duration (s), *M* is the magnitude of the earthquake on the Richter scale that is expected in the area, and *PGA* is the peak ground acceleration given as fractions of g (m s^{-2}).

ND affects the structures when it is in the influence zone of the failure. According to Vega (2013), in the case of regional applications, it is convenient to use Newmark's method with *ND* which corresponds to a measure of total energy absorbed by the ground calculated with a recorded accelerogram (Jibson et al., 1998; Hidalgo, 2013).

Two seismical scenarios were considered in this methodology: the first one uses A_h values obtained from a seismical microzonation of the study area, and the second one uses a uniform A_h value of the study zone obtained from a general seismic hazard study. Dobry duration of 20 s is assumed to represent a critical situation with a magnitude of 7.2 that allows assessing the effect of strong earthquakes with return period greater than 475 years.

To set the failure criterion and the beginning of the movement, it is necessary to set a limit on *ND* that can accumulate the mass of the sliding block like a maximum value when a balance condition does not exist. The critical value adopted for displacement varies widely, as it is highly dependent on a number of parameters such as the type of slope failure, lithology, slope geometry and previous movements on the

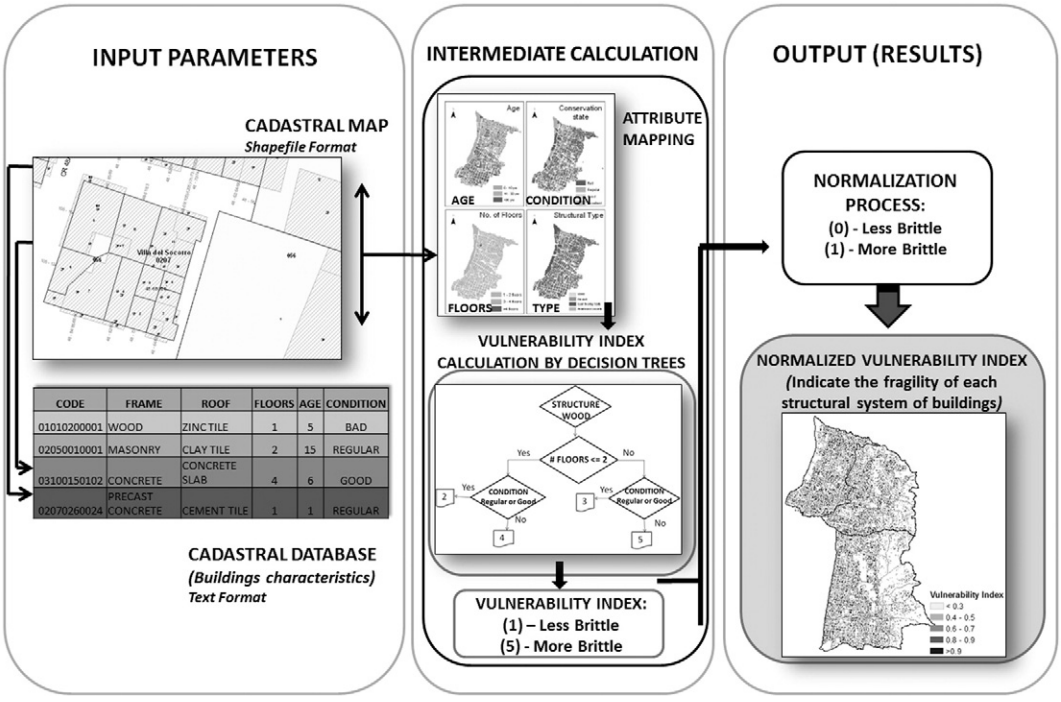

Fig. 2. Schematic methodology adopted for vulnerability assessment.

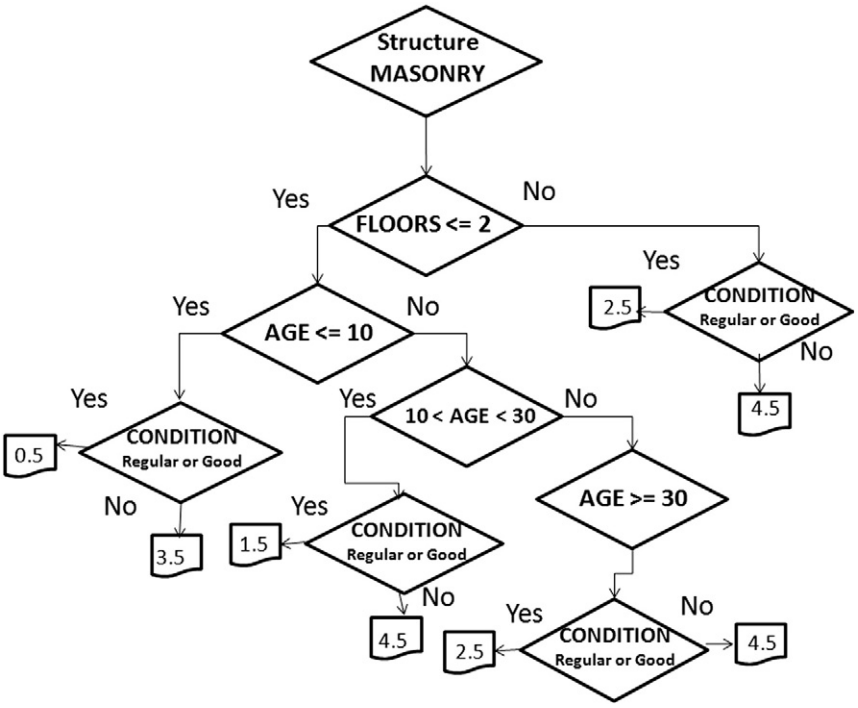

Fig. 3. Decision trees to estimate the vulnerability index for brick structure buildings (with concrete slab cover).

Table 2
Calculation of the vulnerability index for different types of buildings.

Case	Structural System	Number of Floors (Levels)	Age of Construction (years)	Type of Roof	Structural Condition	Vulnerability Index	Normalized Vulnerability Index
1	Scrap Wood	≤2	*	All types	Regular or Good	2	2/5
2	Scrap Wood	≤2	*	All types	Bad	4	4/5
3	Scrap Wood	>2	*	All types	Regular or Good	3	3/5
4	Scrap Wood	>2	*	All types	Bad	5	5/5
5	Precast Concrete	<2	*	All types	Regular or Good	1	1/5
6	Precast Concrete	<2	*	All types	Bad	4	4/5
7	Precast Concrete	≥2	*	All types	Regular or Good	2	2/5
8	Precast Concrete	≥2	*	All types	Bad	5	5/5
9	Masonry (Bricks)	≤2	≤10	Different to Concrete Slab	Regular or Good	1	1/5
10	Masonry (Bricks)	≤2	≤10	Different to Concrete Slab	Bad	4	4/5
11	Masonry (Bricks)	≤2	10 – 30	Different to Concrete Slab	Regular or Good	2	2/5
12	Masonry (Bricks)	≤2	10 – 30	Different to Concrete Slab	Bad	5	5/5
13	Masonry (Bricks)	≤2	≥30	Different to Concrete Slab	Regular or Good	3	3/5
14	Masonry (Bricks)	≤2	≥30	Different to Concrete Slab	Bad	5	5/5
15	Masonry (Bricks)	>2	*	Different to Concrete Slab	Regular or Good	3	3/5
16	Masonry (Bricks)	>2	*	Different to Concrete Slab	Bad	5	5/5
17	Masonry (Bricks)	≤2	≤10	Concrete Slab	Regular or Good	0.5	0.5/5
18	Masonry (Bricks)	≤2	≤10	Concrete Slab	Bad	3.5	3.5/5
19	Masonry (Bricks)	≤2	10 – 30	Concrete Slab	Regular or Good	1.5	1.5/5
20	Masonry (Bricks)	≤2	10 – 30	Concrete Slab	Bad	4.5	4.5/5
21	Masonry (Bricks)	≤2	≥30	Concrete Slab	Regular or Good	2.5	2.5/5
22	Masonry (Bricks)	≤2	≥30	Concrete Slab	Bad	4.5	4.5/5
23	Masonry (Bricks)	>2	*	Concrete Slab	Regular or Good	2.5	2.5/5
24	Masonry (Bricks)	>2	*	Concrete Slab	Bad	4.5	4.5/5
25	Concrete	**	≤10	Different to Concrete Slab	Regular or Good	1	1/5
26	Concrete	**	≤10	Different to Concrete Slab	Bad	5	5/5
27	Concrete	**	10 – 30	Different to Concrete Slab	Regular or Good	2	2/5
28	Concrete	**	10 – 30	Different to Concrete Slab	Bad	5	5/5
29	Concrete	**	≥30	Different to Concrete Slab	Regular or Good	3	3/5
30	Concrete	**	≥30	Different to Concrete Slab	Bad	5	5/5
31	Concrete	**	≤10	Concrete Slab	Regular or Good	0.5	0.5/5
32	Concrete	**	≤10	Concrete Slab	Bad	4.5	4.5/5
33	Concrete	**	10 – 30	Concrete Slab	Regular or Good	1.5	1.5/5
34	Concrete	**	10 – 30	Concrete Slab	Bad	4.5	4.5/5
35	Concrete	**	≥30	Concrete Slab	Regular or Good	2.5	2.5/5
36	Concrete	**	≥30	Concrete Slab	Bad	4.5	4.5/5

* This attribute is not relevant to scrap wood and precast concrete structures.
** This attribute is not relevant to concrete structures.

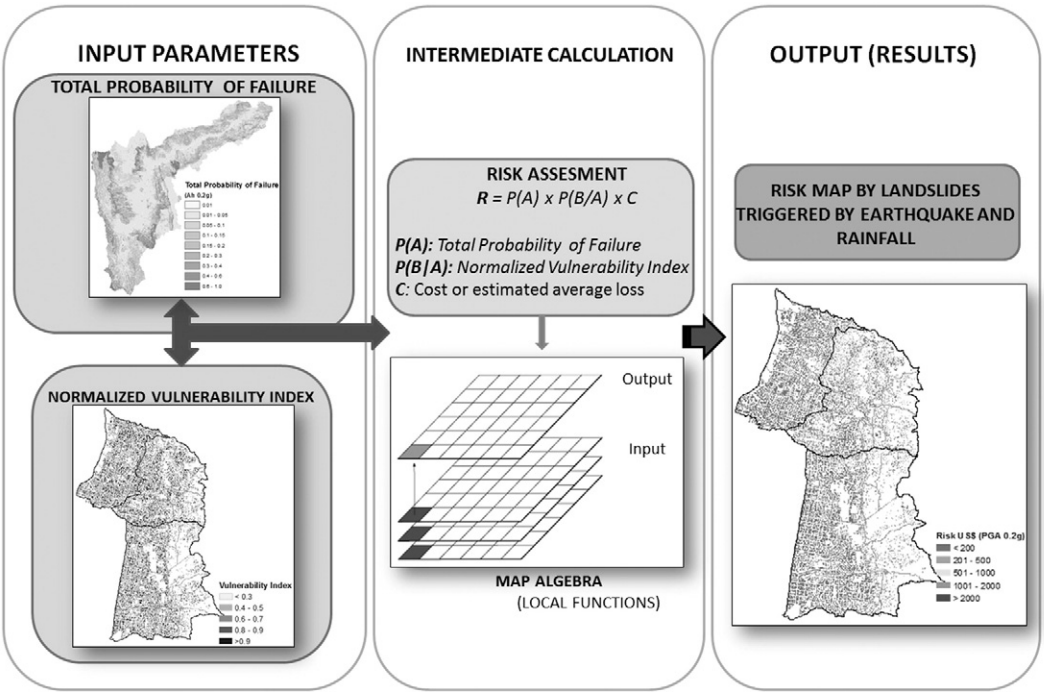

Fig. 4. Schematic methodology adopted to risk assessment.

slope. In general, a displacement larger than 5 cm potentially involves the occurrence of slides, while smaller displacements are common in detachments (Hidalgo, 2013; Chung et al., 2014). Although Newmark's displacements themselves do not represent the exact values of expected deformations, they may be assumed as deformation rates or thresholds representing a condition of stability.

The condition of eventual saturation of the soil is a random phenomenon that must be considered to assess landslide probability. The total probability of landslide is set as:

$$P_{ft} = P_{fs} \times P_s + P_{fns} \times (1 - P_s) \quad (9)$$

where P_{ft} is the probability of total failure, P_{fs} is the probability of failure in a saturated condition resulting from the action of an earthquake, P_{fns} is the probability of failure when the condition is not saturated, and P_s is the marginal probability that the soil is saturated. $(1 - P_s)$ represents the marginal probability that the soil is not saturated.

The probability of failure in saturated and unsaturated conditions can be calculated independently, but it is difficult to determine the probability of soil saturation, due to the complexity and variation of the water content of the soil. However, Moreno et al. (2006) and Hidalgo et al. (2012) indicated that most landslides are caused by soil saturation due to accumulated rainfall, and the occurrence of landslides

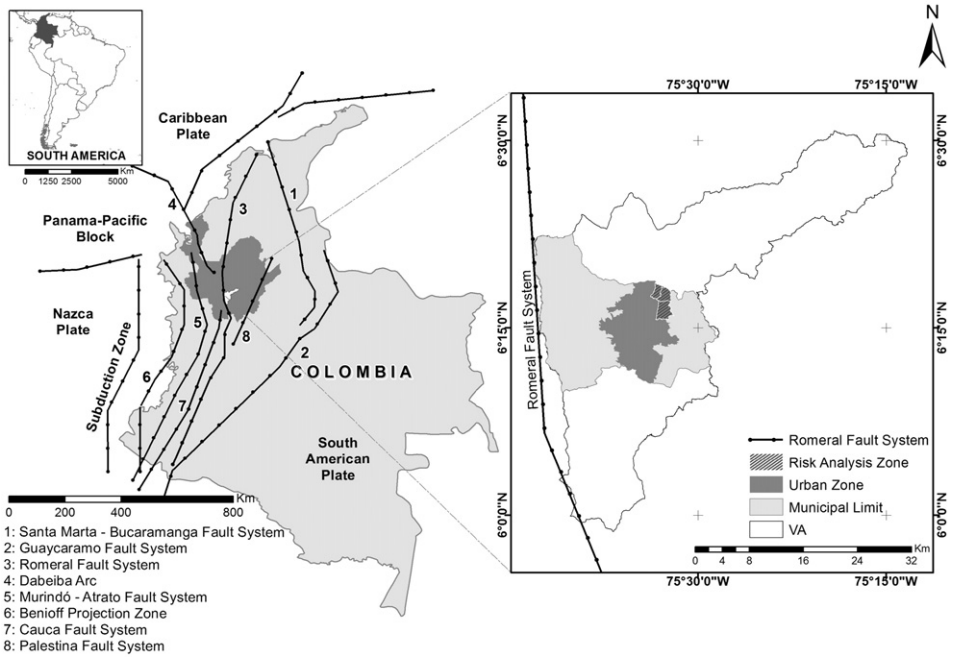

Fig. 5. Location of VA and the study area.

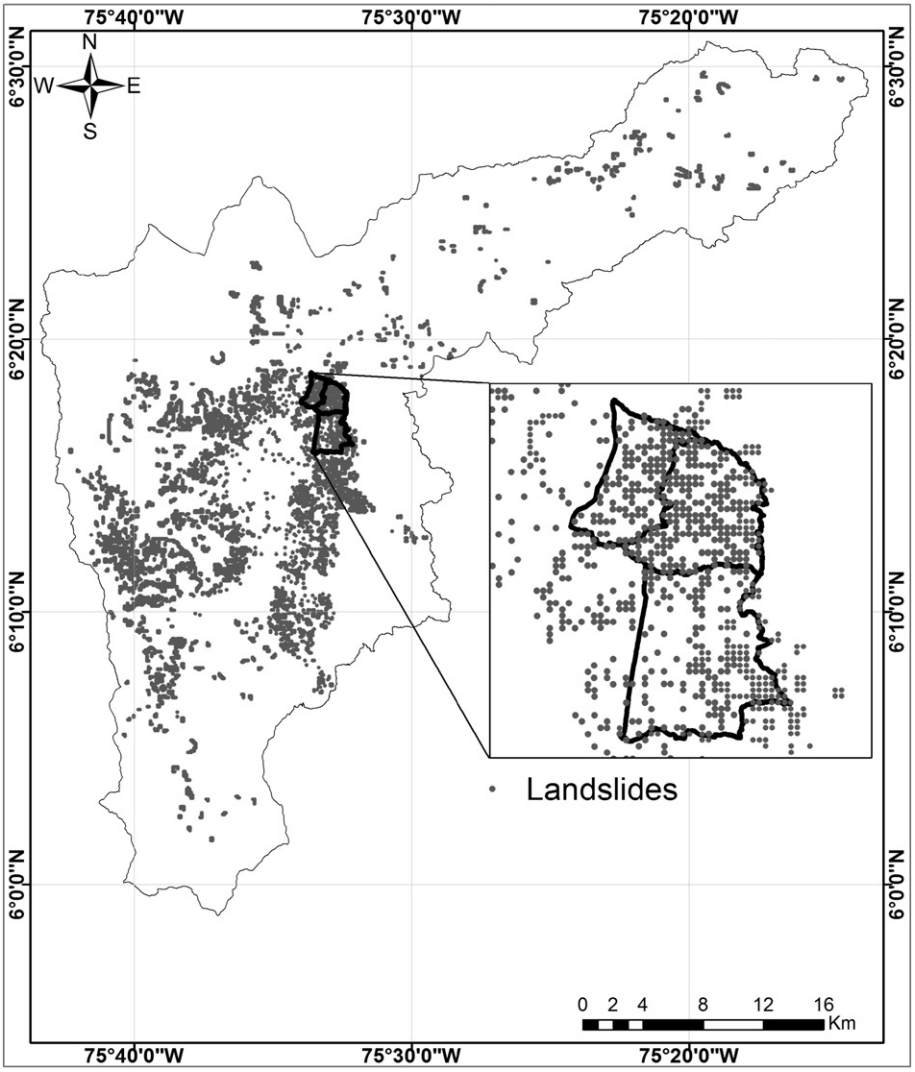

Fig. 6. Landslide inventory (1985–2006).

is related to rainfall amounts or the so-called failure thresholds. This study also assumes that a failure threshold represents a saturation condition that leads to landslides, including a reduction in shear strength due to decreased suction and generation of pressure in pores (Hidalgo et al., 2012; Vega, 2013; Hidalgo, 2013). The probability of saturation is calculated on the basis of the times that previously accumulated rainfall exceeds the failure threshold line in the study area. The failure threshold may be in terms of the previously accumulated rainfall during 3, 5, 15, 30, 60 or 90 days (Aristizábal et al., 2011).

In order to establish the probability of exceeding the threshold, the number of occurrences that the threshold is exceeded is determined and then it is divided by the total number of rainfall records. This means that, according to the methodology used in this study, the soil reached the condition of critical saturation. The return period for these events is calculated using a Gumbel distribution for the acummulated rainfall. After determining the probability that the soil is saturated according to data from climatological stations, a geostatistical interpolation process is developed to estimate the probability of saturation. The interpolation method used in this research was the Kriging method (Vega, 2013), which is an unbiased linear estimator that generates continuous surfaces from precise data, deletes trends of spatial variation as it assumes that it is displayed in the data and provides measures of error.

With the aim of assessing the hazard level, the annual probability of failure is calculated by using the return period of the earthquake and it is classified according to the criteria presented in Table 1. Finally, in order to verify the capacity of the model to determine critical areas, we identified sites with the worst conditions of stability, defined as cells that had a *FOS* of <1.2 in saturated conditions and an acceleration of 0.2 g, and $A_h > A_c$ in saturated conditions, or those that have a major probability of total failure and we compared them with a landslide inventory.

Vulnerability is assessed by using the methodology summarized in Fig. 2. It considers the definition of damage level to buildings with a calculated index using decision trees (Fig. 3). This index is based on the rating of five factors or attributes: the type of structural system, the structural condition (state of conservation), number of floors (levels), type of cover (ceiling), and construction age. These attributes are related to the fragility of the structural system of the buildings to meet the demands in case of a seismic event or a landslide, which reflects the interaction between the type of structure and some of its characteristics. The basic data source for the attributes aforementioned is the municipal cadaster office database. This data is processed to obtain a registration for each building depending on its use and the type of housing and building materials.

Then the database is processed and refined to obtain a unique index that groups the least favorable conditions of each attribute. This is done

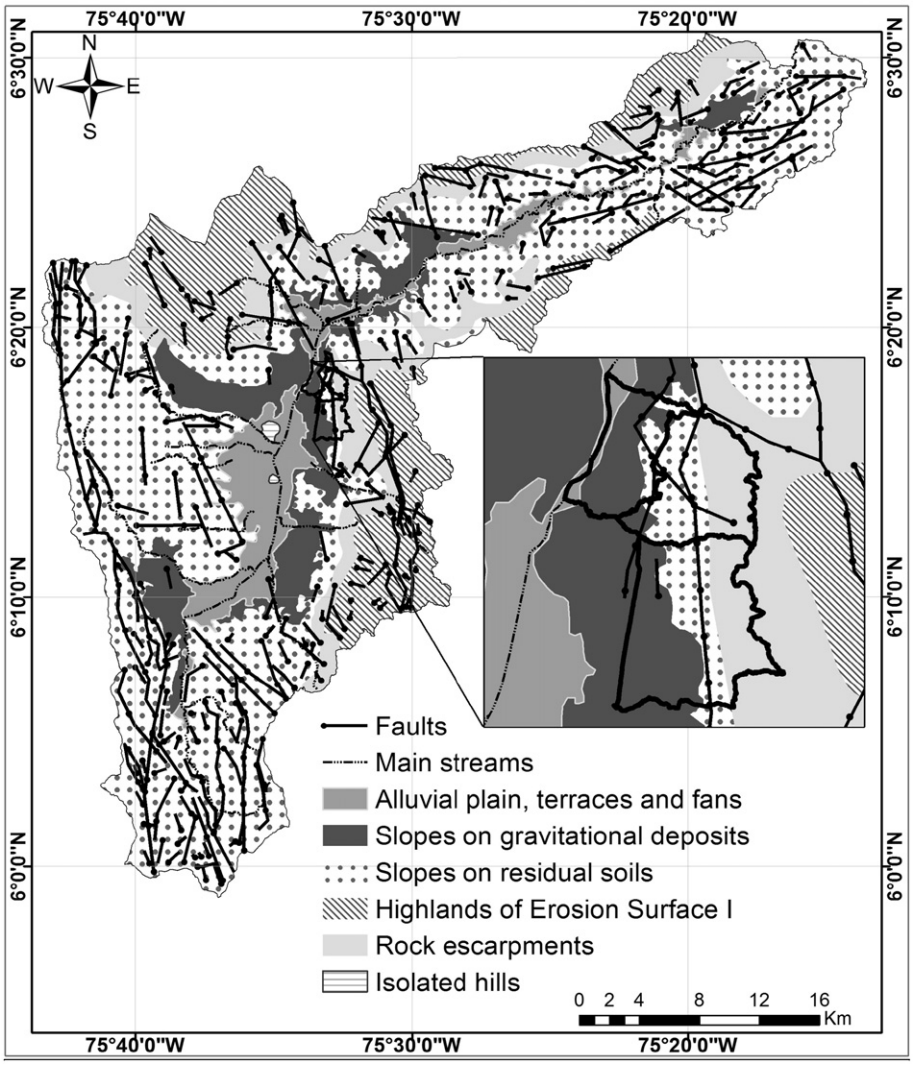

Fig. 7. Geomorphologic map (Modified from AMVA, 2007).

from the vulnerability point of view for each building, considering a scenario where constructions are settled directly on a sliding block or soil mass.

The physical vulnerability indicator of constructions in the study area is calculated by using several decision trees (Fig. 3) and the attributes provided by the Municipal Cadaster Office (MCOM, 2013). Along with these decision trees, a vulnerability index is estimated for each type of building material in the main structure. It allows assigning a value to each variable and to all the combinations in order to reach a final value indicating the level of brittleness and susceptibility to damage of each building. This approach indicates that the lowest value (1) corresponds to the best condition and the highest value (5) corresponds to the worst condition in the least favorable scenario. For example, a two level masonry structure, with less than ten years of age and in good maintenance condition would have a vulnerability index of 1.0. In the case of brick and concrete structural systems with a cover of concrete slab, we have a decrease of 0.5 in the value of the physical vulnerability indicator, obtaining a final result of 0.5 for this indicator as shown in Fig. 3. Therefore, since the diaphragm effect generated by the slab contributed to the rigidity of the structure, it reduced to some extent its fragility or susceptibility to damage. This was taken into account for the structural systems already mentioned, as well as for those with the capacity to support the weight of that type of cover. Once completed, this index was normalized (Fig. 2) to obtain values ranging from zero to one so that it would be compatible with the range used in hazard. Table 2 presents the calculation of the vulnerabiliy index using the rating values for different conditions.

We obtained the risk of damage to buildings in the study area due to a mass landslide triggered by a seismic event through Eq. (1). Consequently, damage indices were estimated as the product of the total probability of failure and the vulnerability index. These indices were calculated considering the costs arising from a potential disaster taking into account house values obtained from cadastral records. The methodology used to estimate landslide risks is summarized in Fig. 4.

A model was developed using Python programming language and ArcGIS™ software for risk calculation, and statistical tools of Excel™ were used to perform data analysis.

Apart from calculating parameters of interest with a value of A_h = 0.2 g, several simulations were performed for other values, i.e. A_h (0 g, 0.05 g, 0.1 g, 0.3 g, 0.5 g, 0.7 g and 1.0 g), in order to model the effect of igniter earthquakes and to analyse the influence and cost variability of probable earthquake-triggered landslides.

3. Case study

The study area is located in the northeastern part of the city of Medellin, centered on the coordinates 6° 15′ N, 75° 35′ W in the central

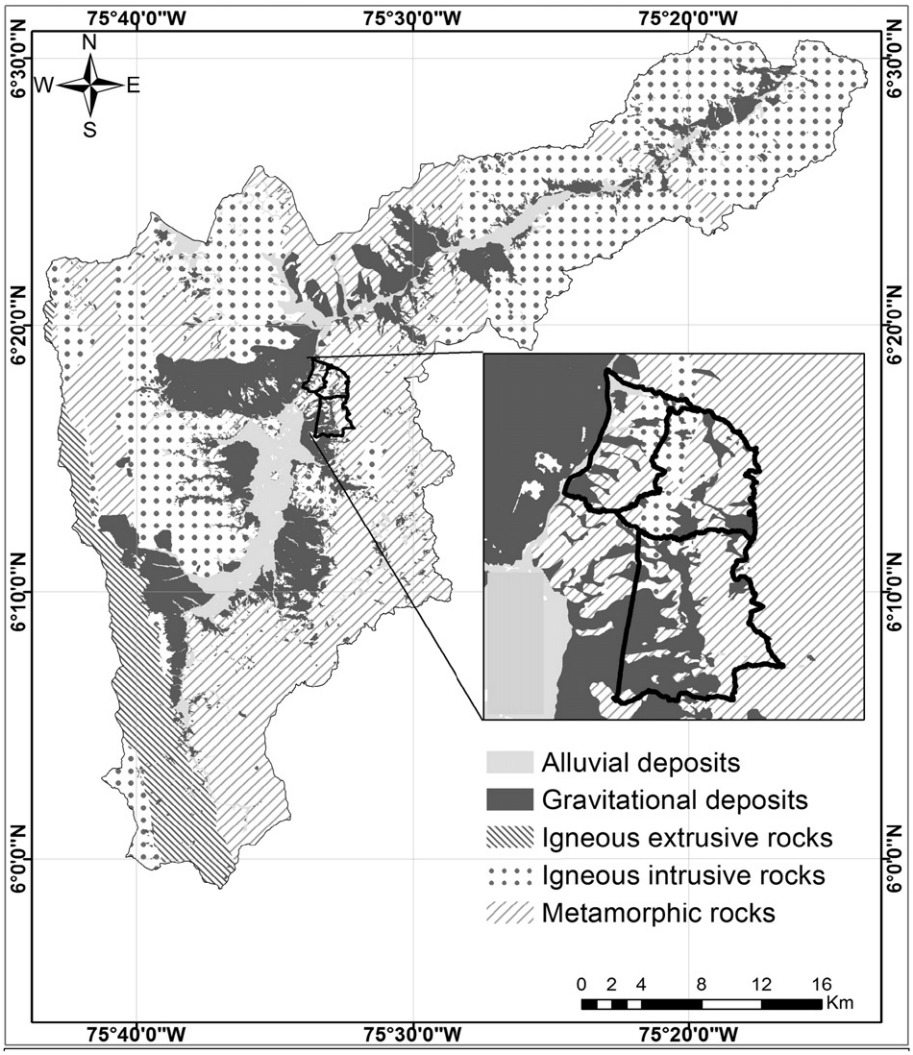

Fig. 8. Geologic map.
(Modified from AMVA, 2007).

part of VA as shown in Fig. 5. This area comprises three groups of neighborhoods called "communes" (i.e. Popular, Santa Cruz and Manrique) with >400,000 inhabitants, settled in an area of 13.4 km^2. In general, the study area is characterized by slopes with gradients of up to 30%, unplanned urbanization, and occasionally there have been incidents caused by landslides. In Fig. 6, the location of landslides registered in the time elapsed from 1985 to 2006 in VA and in the study area are shown. A large concentration of landslides in the study area can be observed in this figure. Although the most recurrent landslides are shallow and triggered by rainfall, deep-seated rotational landslides also occur with a lower frequency but with high impacts, triggered by groundwater flow from adjacent highlands of VA.

Due to the location of the country at the northwestern corner of South America, the study area is situated in a tectonically complex area formed by the confluence of Nazca, South America, Caribbean and Panama plates. This area lies on a bedrock that consists of igneous and metamorphic rocks. In addition, two main fault systems, the Cauca-Romeral and Palestine systems are located close to VA (Fig. 5). Therefore, the study area is exposed to a seismic hazard between middle and high (AMVA, 2007). Geomorphologically, VA may be defined as a tectonic depression that incises an extensive highland partially filled with alluvial deposits from the River Aburra and its tributaries, and deposits originated from ancient landslides and debris flows. The highland incised by VA is composed of two old erosion surfaces. On the other hand, relevant geomorphic units are shown in the geomorphologic map (Fig. 7), i.e. alluvial plains, terraces and fans at the bottom of the valley, slopes on gravitational deposits with a slope gradient between 10 and 30%, slopes on residual soils with a slope gradient between 30 and 50%, isolated hills at the bottom of the valley, rock escarpments in the upper part of the slopes with a slope gradient higher than 50% and highlands with erosion surface I.

In order to identify details on the characteristics of slope and shape of the landscape in the study area and its associated physical processes, a geomorphologic map of a seismic microzonation study to VA (AMVA, 2007) was used. Fig. 7 depicts the categories of different geomorphological units according to criteria of similarity in its geotechnical behavior. The current morphogenetic processes related to relief, climate and geology affect the population of the valley that reached 3.5 million in 2014 and its infrastructure (Vega, 2013). The study area is entirely located on slopes that are underlain by mud and debris flows on slope deposits.

The information required by the model implemented under a GIS environment corresponds to a regular grid of 50 m for each thematic variable. Data used in the model was the one used by Vega (2013), which was extracted mainly from the land use plan of the municipality of Medellín and other studies done by State entities, and it is described below:

3.1. Geological data and soil properties

In VA and the surrounding highlands, there is a varied geology with outcrops of lithological units that include rocks with different ages, origin and composition. Regarding composition, metamorphic rocks such as schist, amphibolites, migmatites and gneisses are considered here, including igneous rocks like granodiorite, dunite, gabbros and basalts; and also sedimentary rocks, alluvial and gravitational deposits (AMVA, 2007).

According to information provided by Hidalgo et al. (2012), Vega (2013), Hidalgo (2013) and Hidalgo and Vega (2014), strength parameters and unit weight were attributed for each of these soils. A denomination for each soil type used in the geological map (Fig. 8) is presented in Table 3, as well as the values of the mean and standard deviation attributed to each parameter compiled by Vega (2013).

3.2. Digital elevation model (DEM)

A model representing the spatial distribution of elevations and topography of the study area (Fig. 9) was used. This layer is a product of a resampling process of other model with better spatial resolution obtained from AMVA (2007). The use of a fifty-meter cell size model was suitable for this study, because the application of a DEM with better resolution for areas with physical soil properties with high uncertainty, would be inefficient as a result of its low cost-benefit ratio (Fuchs et al., 2014). Also it is appropriate for a model of infinite slope like the proposed by Newmark (1965), in which slope length must be much greater than the thickness of the failure zone.

3.3. Seismicity data

The study area is situated in a medium to high seismic hazard prone area because of its geographical position (AIS, 2010), and the origin of its main hazard sources are earthquakes in the subduction zone and in the Cauca-Romeral fault system and other minor fault systems (AMVA, 2007) as shown in Figs. 5 and 7.

In this case, we considered a given distribution of accelerations (A_h) scenario determined by the seismic microzonation of VA (AMVA, 2007) that is displayed in Fig. 9, and a 0.2 g uniform acceleration scenario established by the Colombian building code NSR-10 (AIS, 2010) for the city of Medellin. For the assessment presented in this paper, acceleration was taken on the ground and it was assumed as the product of the rock acceleration. It was done by using a coefficient of importance and a vertical acceleration factor (F_v) in a range between 2 and 4 to consider possible amplifications. These were the result of soil thickness and density for a period of vibration 0, assigned to each cell of the model according to the values determined in NSR-10.

3.4. Rainfall data

Hydrologically, VA is characterized by a bimodal rainfall pattern, with two rainy seasons that occur around March-April-May and September-October-November. The highest values of precipitation are between 2800 and 3200 mm/year and take place in the northern and southern parts of Medellin river basin which crosses longitudinally all the area of VA. Minor precipitation, with values between 1400 and 1800 mm/year, occurs in the central area of the basin and extends toward the west (AMVA, 2009). In Medellin, there is a failure threshold given in terms of the previously accumulated rainfall of 3 (R_3) and 15 days (R_{15}), as follows:

$$R_3 = 110 - 0.5R_{15} \quad (10)$$

Data on daily accumulated precipitation from 10 climatological stations located in VA (Fig. 10) with a series of 13 to 50 years of records was used. Table 4 shows the stations used in this study with geographical location, data period and missing data. The records from each rainfall station were organized and mobile windows from accumulated

Table 3
Properties of Soils (Vega, 2013).

Geologic Unit	Description	Unit Weight (kN/m^3)		Friction Angle (°)		Cohesion (kPa)	
		Mean	Std dev	Mean	Std dev	Mean	Std dev
PZagC	Amphibolite granatifera from Caldas	18.90	0.94	29.90	2.99	34.30	17.15
TRaM	Amphibolites from Medellin	18.90	0.94	29.90	2.99	34.30	17.15
PZaAM	Amphibolites from Alto de Minas	18.90	0.94	29.90	2.99	34.30	17.15
KcdA	Antioquia batholith	18.00	0.90	26.20	2.62	35.50	17.15
Qal	Alluvial deposits	17.70	0.88	29.00	2.90	35.00	17.50
Qat	Torrential alluvial deposits	19.00	0.95	35.00	3.50	12.00	6.00
NFl	Debris and/or sludge flow deposits	14.80	0.74	32.00	3.20	28.40	14.20
JKuM	Dunite from Medellin	16.00	0.80	24.00	2.40	30.00	15.00
TReaB	Amphibole schists of uncultivated	17.60	0.88	27.00	2.70	55.00	27.50
TReC	Schists from Cajamarca	17.60	0.88	27.00	2.70	55.00	27.50
PZeC	Schists from Caldas	17.60	0.88	27.00	2.70	55.00	27.50
KgSD	Gabbro from San Diego	18.10	0.90	33.20	3.32	31.70	15.85
KgC	Gabbros from Copacabana	18.10	0.90	33.20	3.32	31.70	15.85
JgR	Gabbros from Romeral	18.10	0.90	33.20	3.32	31.70	15.85
TRgLC	Gneiss from La Ceja	17.90	0.89	19.00	1.90	16.00	8.00
TRgP	Gneiss from Palmitas	17.90	0.89	19.00	1.90	16.00	8.00
JKgmS	Mylonitic gneisses from Sajonia	17.90	0.89	19.00	1.90	16.00	8.00
Qll	Filled anthropic	19.00	0.95	17.00	1.70	10.00	5.00
JKmbP	Metabasites from Picacho	19.00	0.95	25.00	2.50	22.00	11.00
KvQG	Volcanic member	19.00	0.95	27.00	2.70	30.00	15.00
KvsQG	Member volcano sedimentary	19.00	0.95	24.00	2.40	25.00	12.50
TRmPP	Migmatites from Puente Pelaez	18.50	0.92	27.50	2.75	17.00	8.50
JmI	Mylonite from La Iguana	19.00	0.95	32.00	3.20	16.00	8.00
JuR	Peridotite from Romeral	19.00	0.95	24.00	2.40	30.00	15.00
KdA	Stock Altavista	18.00	0.90	29.00	2.90	19.00	9.50
TRgA	Stock Amaga	18.60	0.93	31.00	3.10	16.00	8.00
KcdE	Stock Las Estancias	18.60	0.93	31.00	3.10	16.00	8.00
KcdML	Stock Media Luna	18.60	0.93	31.00	3.10	16.00	8.00
KtO	Tonalite from Ovejas	18.60	0.93	32.00	3.20	16.00	8.00

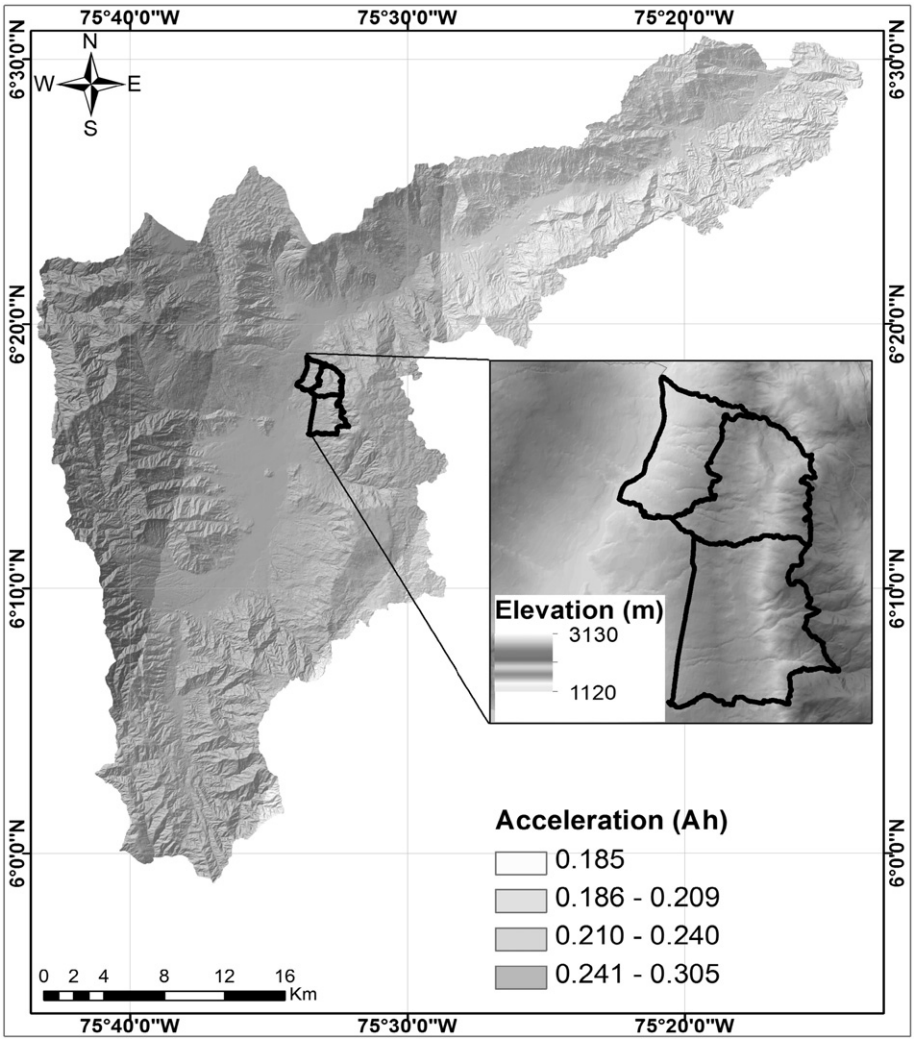

Fig. 9. Map of seismic accelerations and DEM.
(Modified from AMVA, 2007).

rainfall of 3 and 15 days were calculated for each date and were compared with the threshold defined in Eq. 10. Fig. 10 shows the probability distribution of soil saturation in VA obtained by a geostatistical interpolation process in each cell of the model, according to the stations records provided by Hidalgo and Vega (2014). The return period of these events is 2.33 years.

3.5. Cadastral information

In order to estimate the vulnerability index of households, it was necessary to acquire a cartographic database of 48,444 relevant properties (parcels) located in the northeastern zone of the city of Medellin, which represents around 80% of all parcels in the study area. A text file with appropriate alphanumeric information on the structural characteristics of each property was obtained, and it was possible to create a single spatial database. Attributes of the structural system of buildings were used, including age of construction, structural condition, number of floors, type of structural system and type of roof (ceiling), provided by MCOM (2013). Table 5 shows the attributes of each "commune" divided by classes that were obtained using GIS. A map was made for each attribute as shown in Fig. 11 that presents the types of distribution of structural systems as an example; for the sake of brevity the other maps are not shown here.

4. Results

Initially, critical acceleration of each cell was determined taking into account a 5 m-deep surface failure. Critical acceleration in wet conditions ranged from 0 to 1.12 g, and it ranged from 0 to 0.83 g under saturated conditions. With regard to uncertainty, P_{ft} was calculated using Eq. (9); the results obtained are displayed in Fig. 12. It shows a variation between 0.15 and 1.0.

Failure probabilities were obtained for an earthquake with a probability of exceedance of 10% in 50 years, which means that the annual probability of a landslide due to an earthquake ranges from 3×10^{-4} to 2×10^{-3}. According to the distribution of the probabilities of failure and considering the classification in Table 1, 99% of VA territory is under low to very low landslide hazard conditions caused by earthquakes and 1% is under medium hazard conditions. The study area shows that 62% is under very low conditions and 38% is under low conditions.

Fig. 13 shows the results of P_{ft} using Eqs. (2) and (5) for *FOS*, and β coefficient taking values of $A_h = 0.2$ g. P_{ft} values vary between 0.1 and 1.0 with a maximum probability of landslide occurrence of 99.96% in normal conditions of wet soil and 100% in fully saturated soil conditions. Critical points of *FOS* with <1.2 were identified, as shown in Fig. 14. Rectangle A displays the critical points identified in the model and rectangle B shows the records of landslides inventory in the study area.

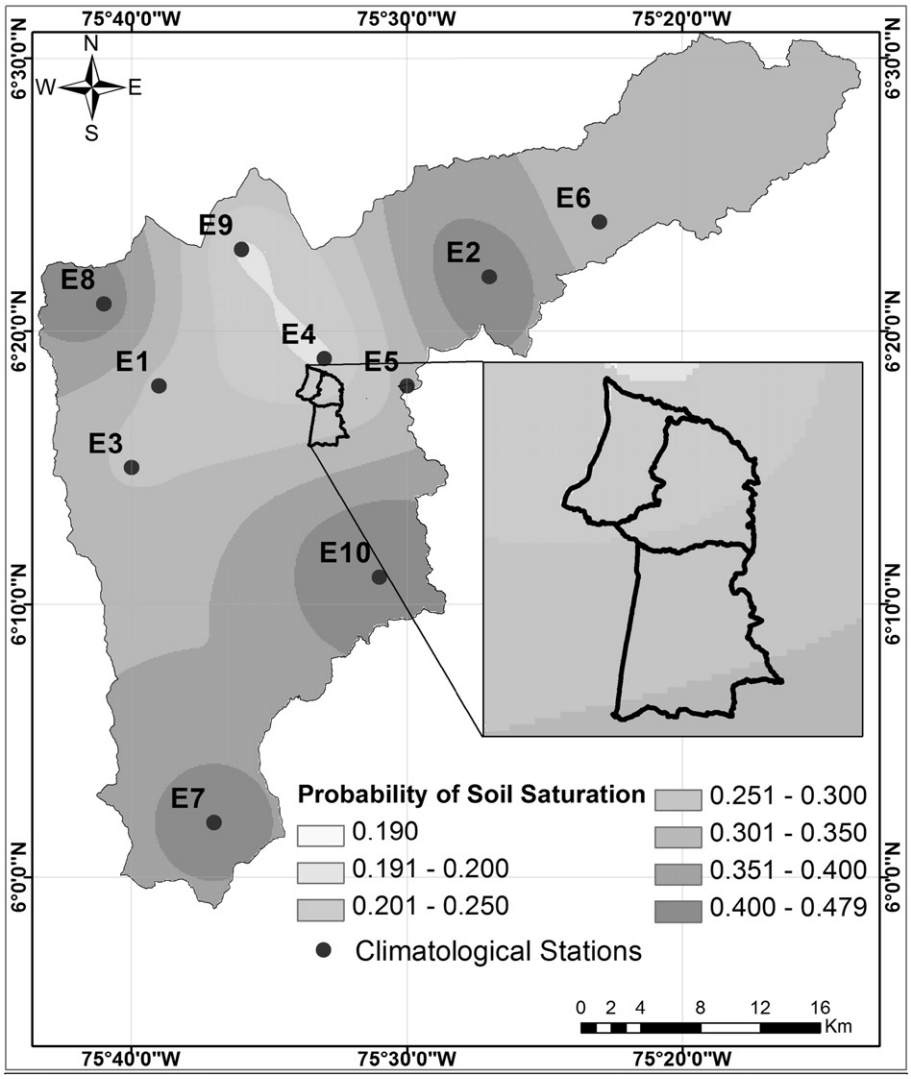

Fig. 10. Probability distribution of soil saturation.
(Modified from Vega, 2013).

Rectangles in Fig. 14 show the areas obtained by a spatial analysis. This analysis calculated critical points with a matching percentage with respect to the inventory in the order of 61% for critical points of *FOS*, representing the normal condition of hillsides. Newmark's displacement *(ND)* was calculated by using Eq. (6) and the results are presented in Fig. 15. The values >5.0 cm are defined as threshold values.

In Fig. 16, the results of the Vulnerability Index are presented. High vulnerability values (showed in dark tones) are displayed on the northeastern sector of the city due to the combined influence of unfavorable conditions for each attribute from the point of view of the structural fragility of the buildings in the study area. The values of the damage index of buildings in the study area are shown in Fig. 17, and risk values of buildings by landslides triggered by earthquakes with $A_h = 0.2$ g and the effect of soil saturation by rainfall are shown in Fig. 18. It is observed that on the eastern side of the study area, the highest values for the risk index are presented, which effectively corresponds to areas with steep slopes and high vulnerability values.

Figs. 19 to 22 illustrate the results of the simulations performed with all A_h values (0 g, 0.05 g, 0.1 g, 0.2 g, 0.3 g, 0.5 g, 0.7 g and 1.0 g), as well as the curves of costs arising from the likelihood of catastrophic events in the study area. These curves consider the maximum estimated loss for different failure rates under the actual structural scenario of buildings, which is called "Scenario 1". These graphs show the expected loss in millions of dollars, for each value of ground acceleration considered in this study. Also, different structural scenarios were evaluated, including: "Scenario 2" that corresponds to a structural type in which masonry was the weakest material, "Scenario 3" consisting of any structural type with stiffening elements, and finally "Scenario 4" that involves a structural type of supporting walls with stiffening elements, which fulfills the minimum structural requirements of Colombian building code – NSR - 10.

Table 4
Climatological stations used in this study. (Modified from Vega, 2013).

Station ID	Station Name	Latitude (N)	Longitude (W)	Data period (Years)	Missing Data (%)
E1	La Iguana	6° 18'	75° 39'	1990–2003	11.5
E2	La Cuchilla	6° 22'	75° 27'	1970–1990	10.8
E3	Astilleros	6° 15'	75° 40'	1991–2003	7.3
E4	Tulio Ospina	6° 19'	75° 33'	1969–2003	7.1
E5	Piedras Blancas	6° 18'	75° 30'	1970–1981	30.1
E6	Hda El Progreso	6° 24'	75° 23'	1973–2003	8.9
E7	La Salada	6° 2'	75° 37'	1984–2004	10.9
E8	Boquerón	6° 21'	75° 41'	1970–1990	11.2
E9	La Meseta Sn Pedro	6° 23'	75° 36'	1970–2004	12.1
E10	Santa Elena	6° 11'	75° 31'	1970–2002	10.7

Table 5
Statistics of attributes evaluated in the study area.

Attribute	Classes	Commune 1		Commune 2		Commune 3		Total Houses	% of Study Zone
Structural Type	Scrap Wood	1652	(9.7%)	815	(6.7%)	831	(4.3%)	3298	6.8%
	Precast Concrete	283	(1.7%)	163	(1.3%)	276	(1.4%)	722	1.5%
	Masonry (Bricks)	10336	(60.9%)	7331	(60.2%)	11007	(57.1%)	28674	59.2%
	Concrete	4700	(27.7%)	3875	(31.8%)	7175	(37.2%)	15750	32.5%
Condition (State of Conservation)	Bad	8765	(51.7%)	6185	(50.8%)	8415	(43.6%)	23365	48.2%
	Regular	8082	(47.6%)	5884	(48.3%)	10777	(55.9%)	24743	51.1%
	Good	107	(0.6%)	96	(0.8%)	92	(0.5%)	295	0.6%
	Excelent	17	(0.1%)	19	(0.2%)	5	(0.0%)	41	0.1%
Number of Floors	Less than or equal 2 levels	15312	(90.2%)	10751	(88.2%)	16932	(87.8%)	42995	88.8%
	3 to 4 levels	1653	(9.7%)	1425	(11.7%)	2348	(12.2%)	5426	11.2%
	Greater than 4 levels	6	(0.0%)	8	(0.1%)	9	(0.1%)	23	0.0%
Age of Construction	Less than or equal 10 years	3618	(21.3%)	1968	(16.2%)	2347	(12.2%)	7933	16.4%
	11 to 30 years	8575	(50.5%)	6678	(54.8%)	11182	(58.0%)	26435	54.6%
	Greater than 30 years	4778	(28.2%)	3538	(29.0%)	5760	(29.9%)	14076	29.0%
Type of Roof	Waste Material	531	(3.1%)	236	(1.9%)	304	(1.6%)	1071	2.2%
	Asbestos-cement Tile	11373	(67.0%)	8001	(65.7%)	12154	(63.0%)	31528	65.1%
	Concrete Slab	4348	(25.6%)	3473	(28.5%)	6173	(32.0%)	13994	28.9%
	Clay Tile	639	(3.8%)	456	(3.7%)	646	(3.4%)	1741	3.6%
	Roof	79	(0.5%)	18	(0.2%)	7	(0.0%)	104	0.2%
	luxurious Roof	1	(0.0%)	0	(0.0%)	5	(0.0%)	6	0.0%
	Total of commune	16971		12184		19289		48444	

Figs. 19 to 22 show that once the peak acceleration of 0.2 g is exceeded with respect to the expected acceleration for the city of Medellin according to the NSR-10, losses have increased considerably with an almost exponential behavior, showing values of up to 1 g. It can be observed that damage begins to be significant in high accelerations of 0.3 g in communes 1 and 3, and 0.4 g in commune 2, which indicates that the level of risk is lower in the latter because it has a lower hazard condition and smaller slope values than other communes. To analyse the effect of ground displacements that exceed the threshold value (5.0 cm) for earthquakes in buildings of the study area, an estimated loss was quantified according to a normalized vulnerability index. We can observe that the buildings with a high level of fragility are the most affected by landslides with an *ND* higher than the threshold value. The quantification of estimated losses can be seen in Fig. 23.

5. Discussion

The model developed in this study allows an estimation of risk in the influence zone of earthquake-triggered landslides including the influence of saturation conditions due to rainfall. Our results show that the model is sufficiently robust to identify critical areas for stability. Furthermore, it is possible to study in detail the prioritization of areas to ensure the safety of people and infrastructure in the vicinity of the site.

Since most data were obtained from secondary sources, this is an economic methodology that provides a basis for decision-making in the planning process of large areas and the prioritization of areas requiring further study. This is an important feature of the methodology for use in developing countries where the greatest human losses due to landslides occur (Kirschbaum et al., 2015). The probabilistic approach used in this study enables the incorporation of uncertainty in the analyses.

With the critical points determined by the model, we found that there is an incidence and correlation between geomorphology and structural geology in the study area. The landforms and the distinctive erosion and escarpment of the eastern hillside of VA influence the stability of the hillsides in the study area. The most critical areas were characterized by slopes >40% (22°) and unfavorable hydrological conditions, such as the northwest and southeast zones of the VA, where we estimated probabilities of saturation higher than 40%. This is logical considering

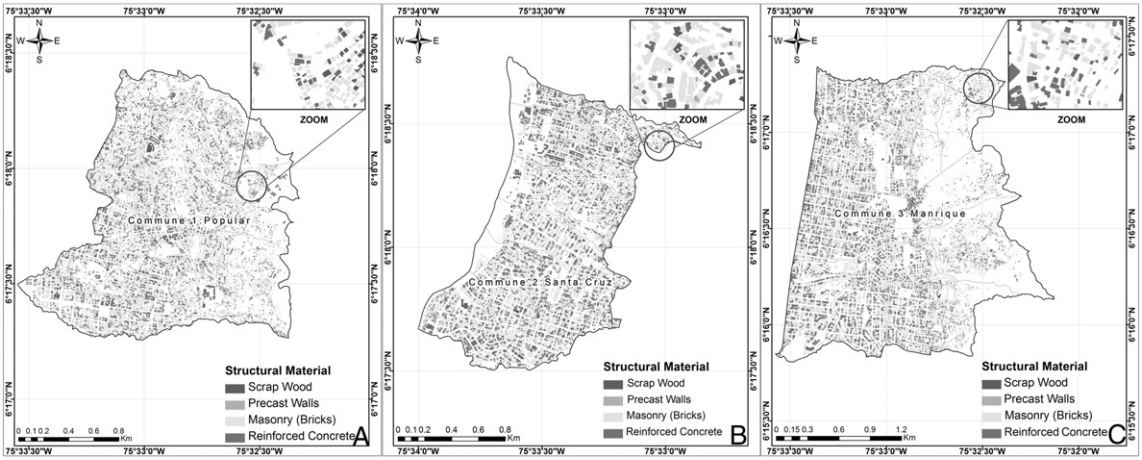

Fig. 11. Types of structural systems (Frames) of buildings: A) commune 1-Popular, B) commune 2-Santa Cruz, C) commune 3-Manrique.

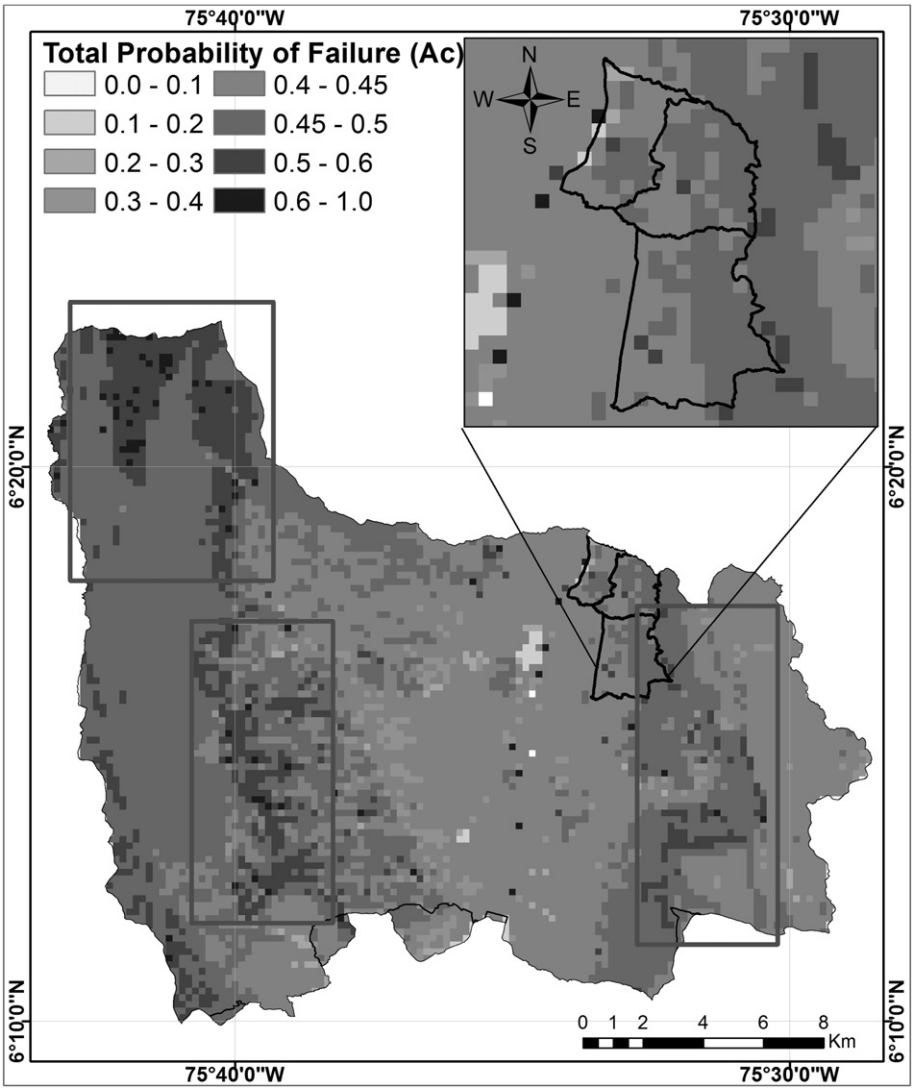

Fig. 12. Distribution of total probability of failure $P(A_h > A_c)$.

that has been verified the influence of saturation on increasing pore pressure (Ali et al., 2014). In contrast, the less hazardous areas were those with gentler slopes (with <40%) located in the central zone of VA. These areas have 0.4–0.5 failure probabilities and represent approximately 86% of the study area. For future work we will simulate the infiltration process, which has been identified as a very important variable for the occurrence of shallow landslides triggered by earthquakes (Chen and Zhang, 2014).

P_{tf} obtained in terms of *FOS* had a similar distribution to the one observed in A_c. In both cases, the most unfavorable conditions were found in the northwest zone of the jurisdiction of Palmitas and in the southeastern part of VA (highlighted with boxes in Fig. 14), and the most stable conditions were observed in the central area. The range of values of failure probabilities and its distribution are comparable to other methodologies used in previous studies (AMVA, 2009). Moreover, it shows that low and very low levels of landslide hazards are predominant in the study area and that medium and high levels only appear in areas with steeper slopes.

P_{tf} obtained in terms of *DN* showed a marked tendency with values above the threshold, in a northeast direction, which is associated with some features of the territory in terms of geomorphology, slope, local materials and its geomechanical parameters (Fig. 15). Special emphasis is placed on the boxes marked in this figure, in which there is a correlation >5.0 cm in displacements with high failure probability values obtained for both A_c and $A_h = 0.2$ g. As shown in this figure, the premise that a saturation state of the soil establishes an adverse condition on slopes is validated, so displacements obtained after the action of the earthquake are higher than in natural or wet soil conditions.

From the analysis of losses arising from damages to buildings in the study area that we performed under different scenarios and structural conditions, it was found that under an assumed scenario in which all the constructions of the study area fulfill the requirements of the Colombian buiding code (NSR-10), there is a decrease in costs related to the effect of landslides disasters of approximately 63%. This is compared to the condition of the actual structural scenario for the maximum horizontal acceleration of the ground expected in the city, which is an earthquake with a 475-year return period, according to a 2002 study of seismic microzonation. We found that the improvement of the structural quality of buildings has a major effect on estimated costs of damage, as it may decrease between US$50 and US$100 million depending on the earthquake recurrence period even without the full implementation of the NSR-10. Vulnerability index represents a way to incorporate uncertainty associated

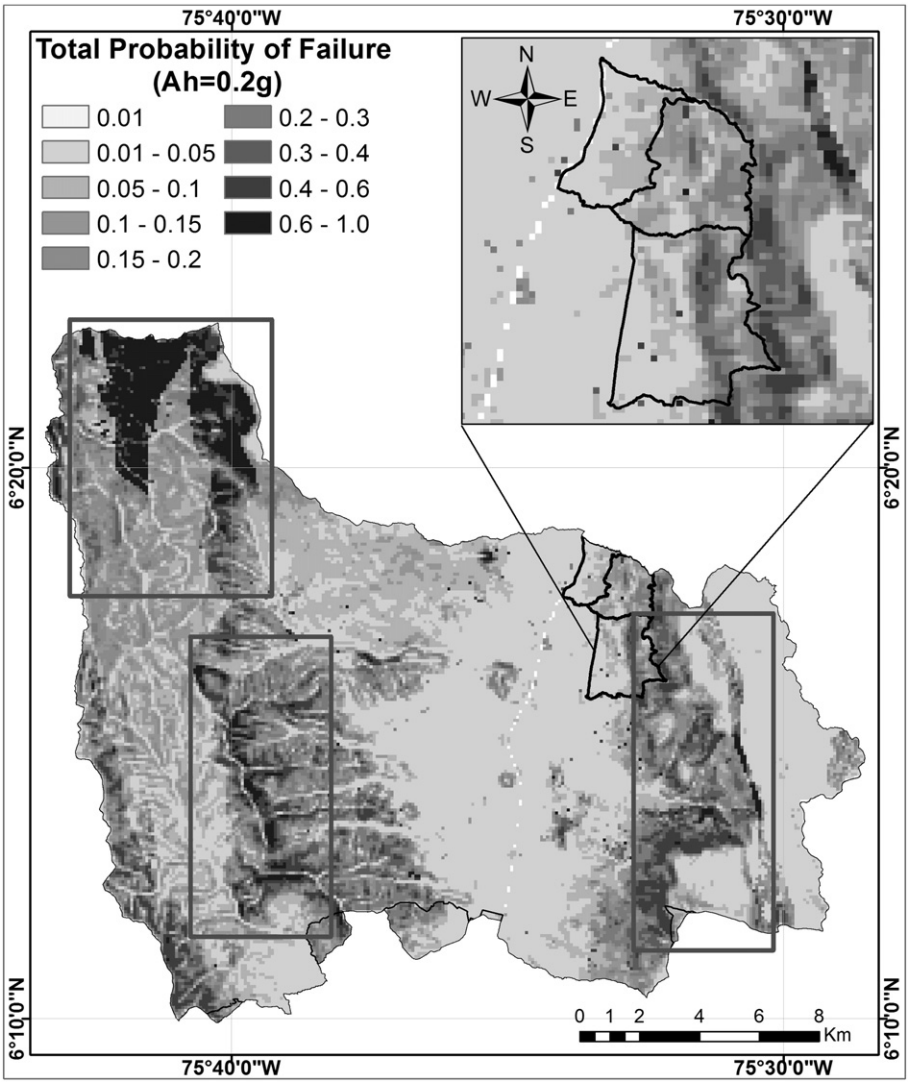

Fig. 13. Distribution of total probability of failure for P($FOS < 1$) with $A_h = 0.2$ g.

with vulnerability assessment, which is not feasible to be fully due to lack of data and the subjectivity of the required parameters (Uzielli et al., 2008).

Because of the way data were obtained, mostly from secondary sources, uncertainty levels are high. However, the probabilistic approach used enables us to incorporate uncertainty in the analyses. In this case, the major source of uncertainty is epistemic because there is uncertainty in site characterization, models and parameters. The uncertainty in site characterization depends on the proper interpretation given to the stratigraphic profiles, resulting in uncertainty of exploration and data, including measurement errors, inconsistency and heterogeneity of data, handling of data and transcription errors. This uncertainty was covered by wide ranges of variation as shown in Table 3. The uncertainty of the models depends on the level of precision in which the mathematical model represents reality. Moreover, the uncertainty derived from the parameters depends on the accuracy of the estimation of model parameters. The inaccuracy of the parameter values that resulted from test or calibration data is increased by a limited number of observations. This is covered by probabilistic assessments with varying parameters in wide ranges such as the characterization of uncertainty. Regarding the sources of uncertainty, we noted that DEM was generated from a photogrammetric restitution, so the altimetry precision and its derivative products like the slope map are also conditioned by the process of generation. About precipitation data, we noticed that one of the 10 climatological stations used for analyses, the one closest to the study area (station Piedras Blancas) had the highest percentage of missing data, then interpolated values within the study area may have high uncertainty. The use of decision trees has the limitation that they are not associated with any action related to a particular phenomenon, so it is considered a generic level of damage. Cadastral data were obtained through a property census done house by house, so this information is presumed to be accurate.

6. Conclusions

The model developed in this study allows a hazard assessment in the influence zone of earthquake and rainfall triggered landslides while considering uncertainties about soil strength, and rainfall and earthquake occurrence. This research shows that the model is capable of identifying critical areas of stability for prioritization of hazard mitigation programs. The model also performs an estimation of the vulnerability of buildings in the influence zone using the structural characteristics and direct costs with data obtained from secondary sources. Therefore, it allows different seismic and structural scenarios to be evaluated economically, and provides a basis for the

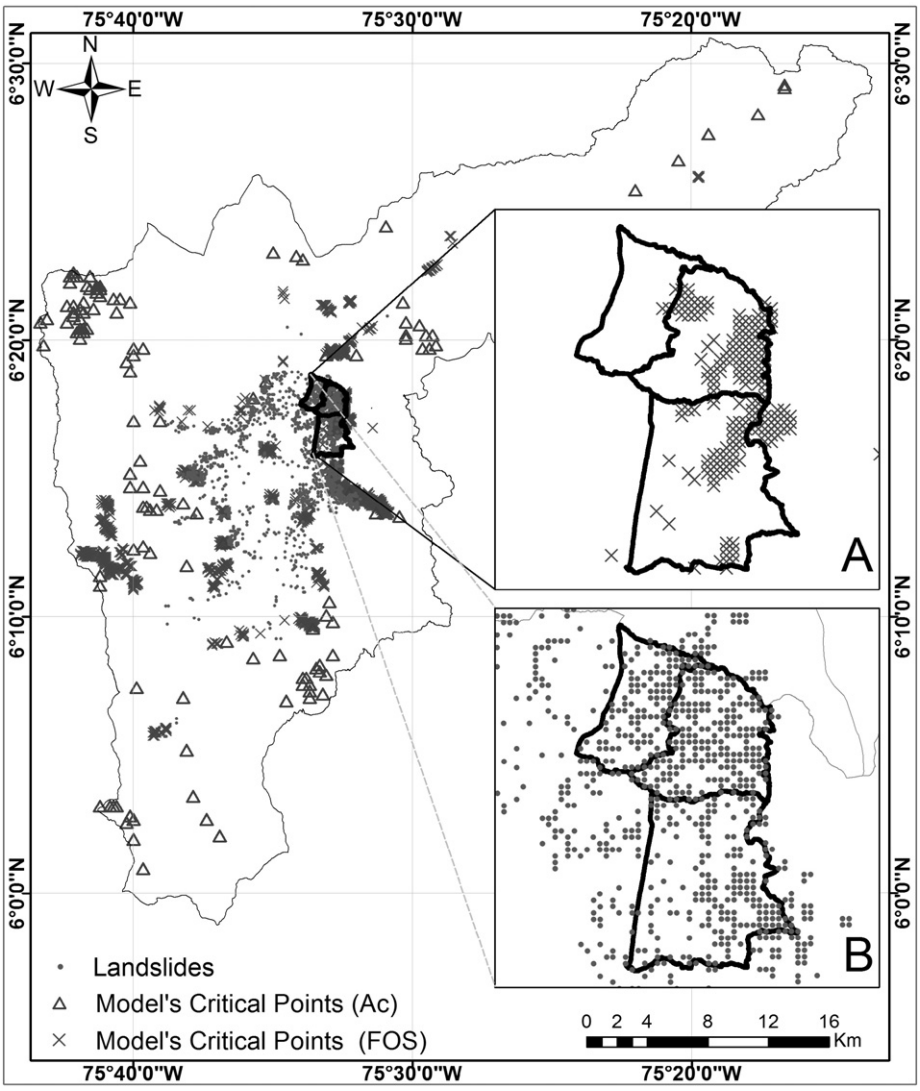

Fig. 14. Location of critical points in the study area.

decision-making stage of the planning process of large areas and the prioritization of areas requiring further study.

Mass movements of soil are likely to occur if an earthquake has the characteristics prescribed in VA by this study, and this probability may increased if soils are saturated. The actual conditions show that 99% of VA is under very low condition of landslide hazard while 62% of the study area is under low hazard condition and 38% is under very low condition. Furthermore, losses caused by earthquake and rainfall triggered landslides are significant with accelerations >0.3 g. In the case of lower accelerations, the affected areas are those with steeper slopes with poor quality housing construction, mostly made of wood. It is possible to determine the amount of investment required to reduce the risk of buildings exposed to a disastrous event to an acceptable level of safety through cost analysis. For example, for the same value of A_h it is possible to estimate the maximum expected cost for a city in a given return period, as the difference in cost between the actual structural scenario of exposed buildings and an assumed scenario that fulfills regulations about seismic resistant constructions. This improvement in building constructions generates a decrease in losses of 63%.

The methodology developed in this study may serve as a basis for the implementation of a landslide warning system built on physically based models and hazard assessments, being able to establish a zonification in terms of the annual probability of occurrence of landslides. However, it is necessary to develop new analyses that allow the inclusion of a larger amount of rainfall data, the modeling of water flow within the soil mass and earthquakes with different periods of recurrence, since this work was limited to earthquakes with return periods of 475 years. Similarly, the calculation of vulnerability indices from fragility curves representing the probability that a structure is in a specific state of damage to a given level of demand is intended to be used later.

Acknowledgements

We thank the editor, Takashi Oguchi, and all reviewers for their constructive comments and suggestions that helped to improve this paper. We would like to extend our sincerest gratitude to the Municipal Cadastre Office of Medellín City for their cooperation during this research.

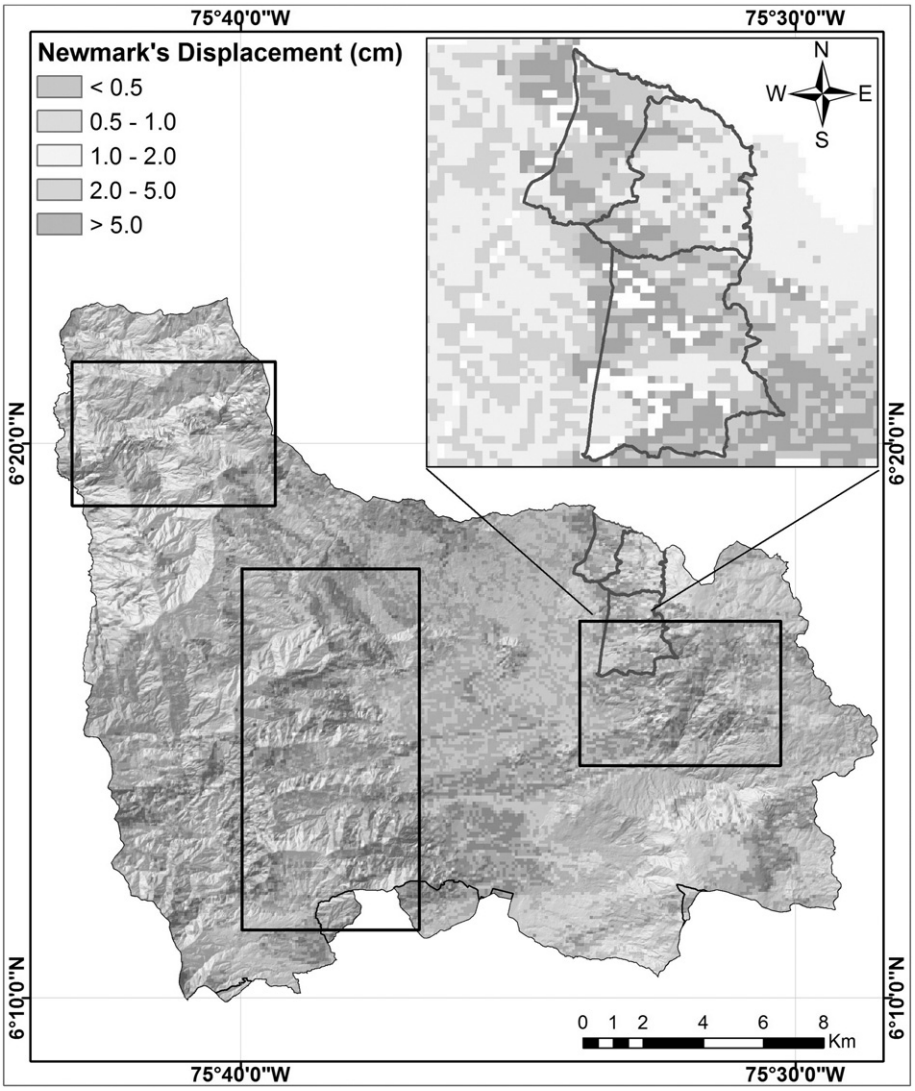

Fig. 15. Newmark's displacement.

Fig. 16. Vulnerability index of buildings: A) commune 1-Popular, B) commune 2-Santa Cruz, C) commune 3-Manrique.

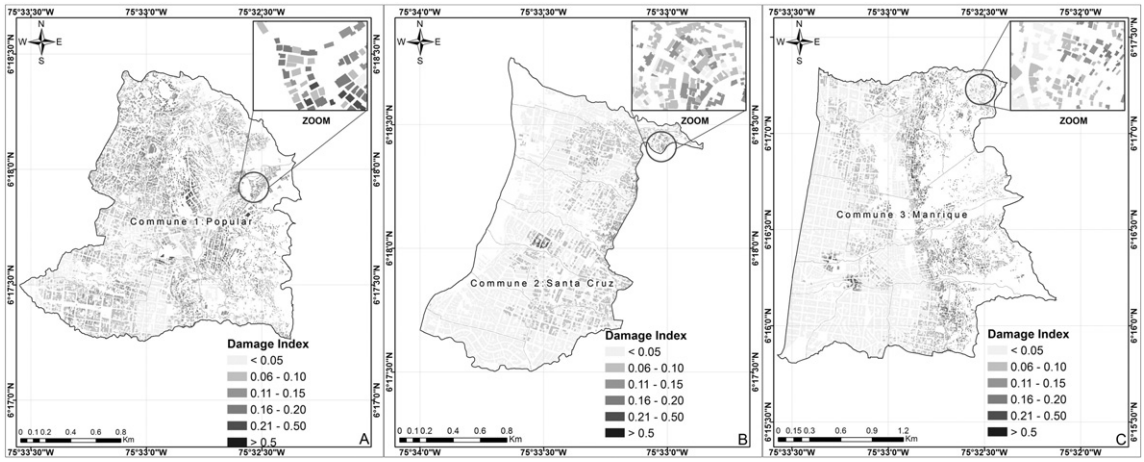

Fig. 17. Damage Index of buildings:: A) commune 1-Popular, B) commune 2-Santa Cruz, C) commune 3-Manrique.

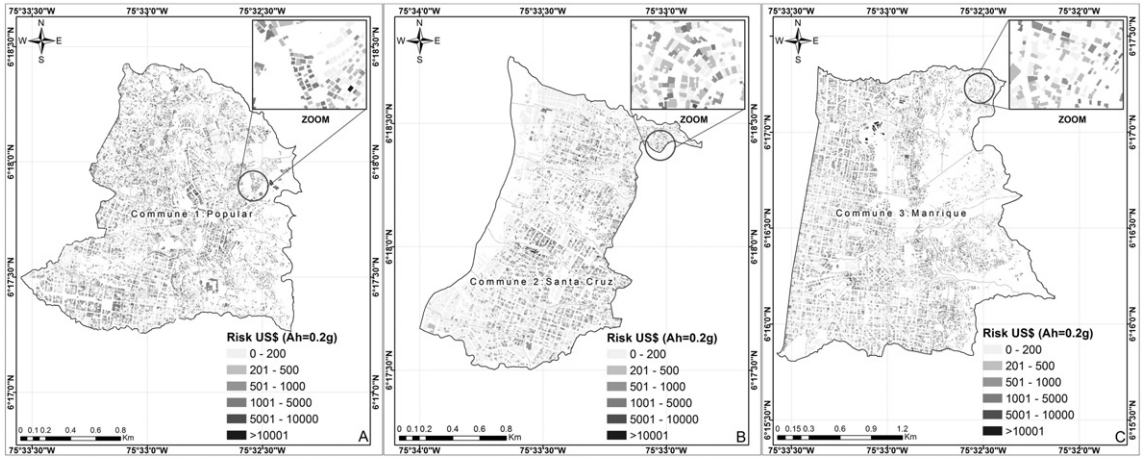

Fig. 18. Risk of buildings:: A) commune 1-Popular, B) commune 2-Santa Cruz, C) commune 3-Manrique.

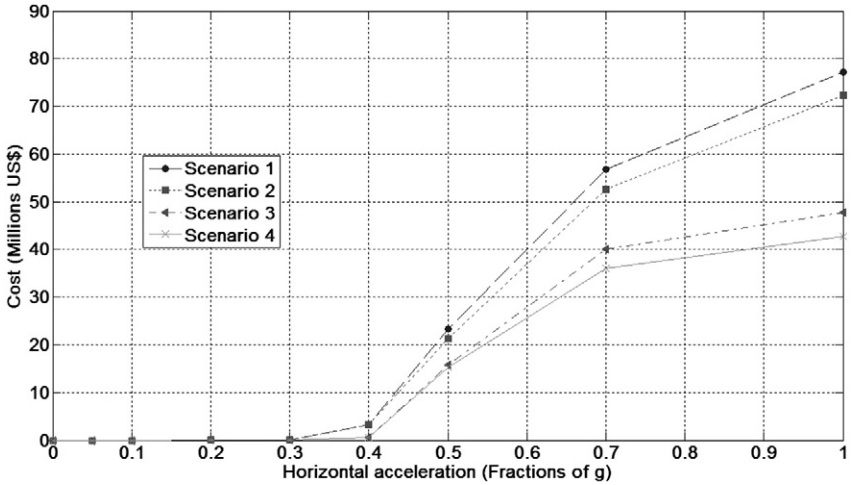

Fig. 19. Probable maximum loss for a damage index higher than 50% to different structural scenarios in Commune 1.

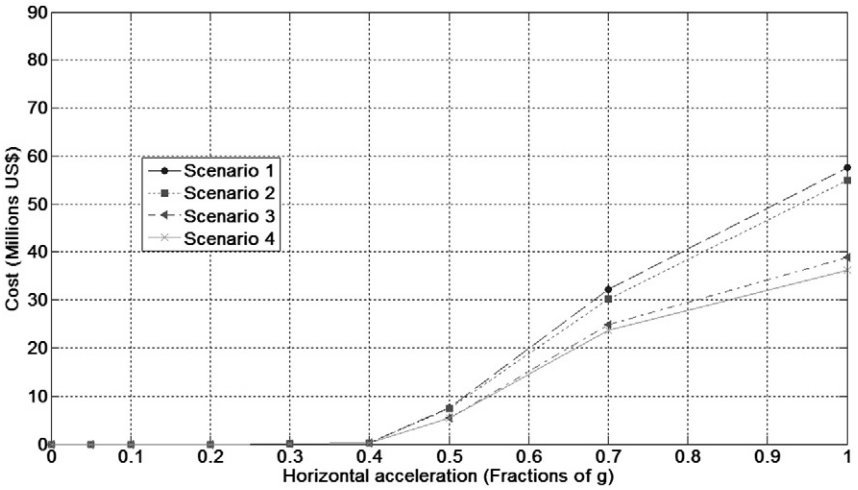

Fig. 20. Probable maximum loss for a damage index higher than 50% to different structural scenarios in Commune 2.

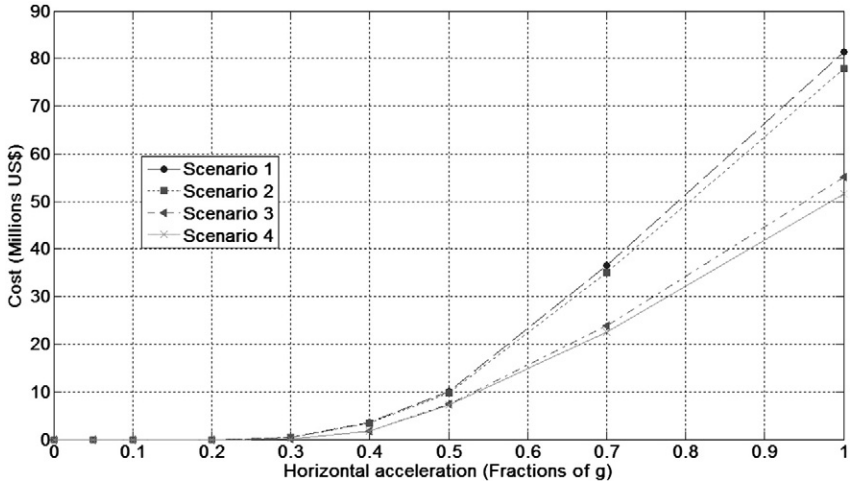

Fig. 21. Probable maximum loss for a damage index higher than 50% to different structural scenarios in Commune 3.

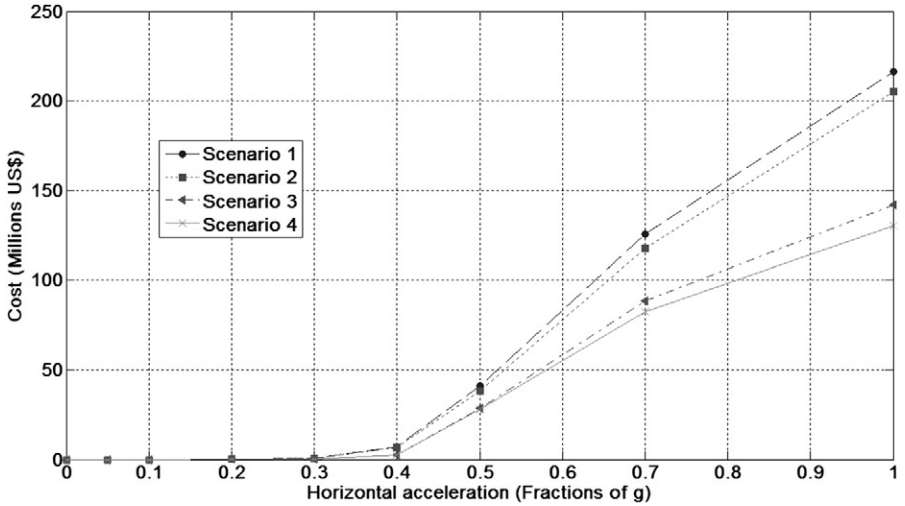

Fig. 22. Probable maximum loss for a damage index higher than 50% to different structural scenarios in the study area.

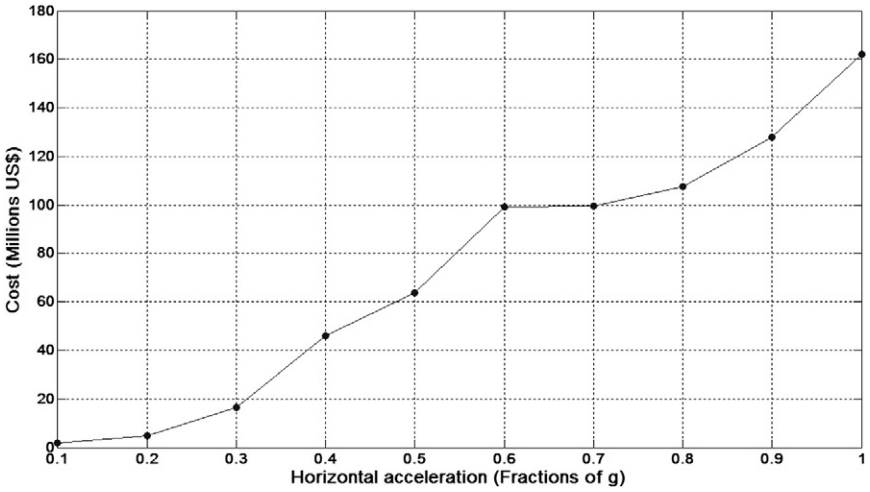

Fig. 23. Estimated Loss in relation to vulnerability index for areas with *ND* >5.0 cm.

References

AIS, 2010. Colombian Code for Earthquake-resistant Construction (NSR-10). Association of Earthquake Engineering, Colombia (In Spanish).

Ali, A., Huang, J., Lyamin, A.V., Sloan, S.W., Griffiths, D.V., Cassidy, M.J., Li, J.H., 2014. Simplified quantitative risk assessment of rainfall-induced landslides modelled by infinite slopes. Eng. Geol. 179, 102–116.

AMVA, 2007. Microzonation and assessment seismic risk in Valle de Aburrá. Metropolitan Area of Valle de Aburrá 29. Institutional Publication (In Spanish). (184 pp.).

AMVA, 2009. Joint Project with the municipalities of Medellin and Envigado, Corantioquia and the National University of Colombia. "Hazard, Vulnerability and Risk for Landslides, Torrential Floods and Floods in the Valle de Aburrá. Formulation of Management Proposals. (In Spanish). Metropolitan Area of Valle de Aburrá. Book II (225 pp.).

Aristizábal, E., Gamboa, M., Leoz, F., 2010. Early warning system for mass movements triggered by rainfall in the Valle de Aburrá, Colombia. (in Spanish). Rev. EIA 13, 155–169.

Aristizábal, E., González, T., Montoya, J.D., Vélez, J.I., Martínez, H., Guerra, A., 2011. Analysis of empirical rainfall thresholds for the prognosis of landslides in the Aburrá Valley, Colombia. (in Spanish). Rev. EIA 15, 95–111.

Baecher, G.B., Christian, J.T., 2003. Reliability and Statistics in Geotechnical Engineering. John Wiley & Sons, England (620 pp.).

Bonachea, J., 2006. Development, Implementation and Validation of Methods and Models for Assessment of Hazards, Vulnerability and Risk due to Geomorphological Processes. (In Spanish) (Doctoral Dissertation) Science Faculty. Department of Earth Sciences and Physics of Condensed Matter. University of Cantabria, Santander, Spain (278 pp.).

Borgomeo, E., Hebditch, K., Whittaker, A., Lonergan, L., 2014. Characterising the spatial distribution, frequency and geomorphic controls on landslide occurrence, Molise, Italy. Geomorphology 226, 148–161.

Botero, V., 2009. Geo-information for measuring vulnerability to earthquakes: a fitness for use approach (Doctoral Dissertation) International Institute for Geo-information Science and Earth Observation. University of Utrecht, Netherlands (212 pp.).

Campos, A., Holm-Nielsen, N., Díaz, C., Rubiano, D., Costa, C., Ramirez, F., Dickson, E., 2012. Analysis of Disaster Risk Management in Colombia. A Contribution for the Construction of Public Policies (In Spanish) World Bank, Bogota, Colombia (436 pp.).

Chen, H.X., Zhang, L.M., 2014. A physically-based distributed cell model for predicting regional rainfall-induced shallow slope failures. Eng. Geol. 176, 79–92.

Chen, X.L., Liu, C.G., Yu, L., Lin, C.X., 2014. Critical acceleration as a criterion in seismic landslide susceptibility assessment. Geomorphology 217, 15–22.

Chowdhury, R., Flentje, P., Bhattacharya, G., 2010. Geotechnical Slope Analysis. Taylor & Francis, England (737 pp.).

Christian, J.T., Ladd, C.C., Baecher, G.B., 1994. Reliability applied to slope stability analysis. J. Geotech. Eng. 120, 2180–2207.

Chung, J., Rogers, J.D., Watkins, C.M., 2014. Estimating severity of seismically induced landslides and lateral spreads using threshold water levels. Geomorphology 204, 31–41.

Dragicevic, S., Lai, T., Balram, S., 2015. GIS-based multicriteria evaluation with multiscale analysis to characterize urban landslide susceptibility in data-scarce environments. Habitat International. Special Issue: Exploratory Spatial Analysis of Urban Habitats 45 Part 2, pp. 114–125.

Epifânio, B., Zêzere, J.J., Neves, M., 2014. Susceptibility assessment to different types of landslides in the coastal cliffs of Lourinhã (Central Portugal). J. Sea Res. 93, 150–159.

Faraji Sabokbar, H., Shadman Roodposhti, M., Tazik, E., 2014. Landslide susceptibility mapping using geographically-weighted principal component analysis. Geomorphology 226, 15–24.

Fuchs, M., Torizin, J., Kühn, F., 2014. The effect of DEM resolution on the computation of the factor of safety using an infinite slope model. Geomorphology 22, 416–426.

Hidalgo, C.A., 2013. Uncertainty, Vulnerability and Risk Assessment Due to landslide on Roads. (In Portuguese) (Doctoral Tesis) Department of Civil and Environmental Engineering, University of Brasilia, Brasil (250 pp.).

Hidalgo, C.A., Vega, J.A., 2014. Estimation of earthquake triggered landslides hazard (Aburrá Valley-Colombia). (in Spanish). Rev. EIA 11 (22), 103–117.

Hidalgo, C.A., Vega, J.A., Assis, A., 2012. Estimating landslide hazard in linear projects: Roads in residual soils". (In Spanish). Proceedings of the Fourth Panamerican Symposium of landslide - IVSPD, Colombian Geotechnical Society, Paipa, Colombia.

Jaiswal, P., Van Westen, C.J., 2009. Estimating temporal probability for landslide initiation along transportation routes based on rainfall thresholds. Geomorphology 112, 96–105.

Jaiswal, P., Van Westen, C.J., Jetten, V., 2010. Quantitative landslide hazard assessment along a transportation corridor in southern India. Eng. Geol. 116, 236–250.

Jibson, R.W., Harp, E.L., Michael, J.A., 1998. A method for producing digital probabilistic seismic landslide hazard maps. Eng. Geol. 58, 271–289.

Kirschbaum, D., Stanley, T., Zhoua, Y., 2015. Spatial and temporal analysis of a global landslide catalog. Geomorphology 249, 4–15.

Mancini, F., Ceppi, C., Ritrovato, G., 2010. GIS and statistical analysis for landslide susceptibility mapping in the Daunia area, Italy. Nat. Hazards Earth Syst. Sci. 10, 1851–1864.

Martha, T.R., Van Westen, C.J., Kerle, N., Jetten, V., Vinod Kumar, K., 2013. Landslide hazard and risk assessment using semi-automatically created landslide inventories. Geomorphology 184, 139–150.

MCOM, 2013. Cadastral Inventory Geodatabase. Municipal Cadastral Office of Medellín City.

Moreno, H.A., Vélez, M.A., Montoya, J.D., 2006. The rainfall and landslides in Antioquia: analysis of its occurrence in the year, intra-annual and daily scales. (in Spanish). Rev. EIA 5, 59–69.

Newmark, N., 1965. Effects of earthquakes on dams and embankments. Géotechnique 15, 139–159.

Panahi, M., Damavandi, A., Rezaiee, F., Panahi, S., 2011. GIS-based earthquake vulnerability of schools in district one of Tehran Municipality using Analytical Hierarchy Process. Proceedings of the International Annual Conference on Geo-Information for Disaster Management (Gi4DM). International Society of Photogrammetry and Remote Sensing (ISPRS), Antalya, Turkey.

Promper, C., Puissant, A., Malet, J.P., Glade, T., 2014. Analysis of land cover changes in the past and the future as contribution to landslide risk scenarios. Appl. Geogr. 53, 11–19.

Remondo, J., Bonachea, J., Cendrero, A., 2008. Quantitative landslide risk assessment and mapping on the basis of recent occurrences. Geomorphology 94 (3–4), 496–507.

Saboya, F., Alves, M., Pinto, W., 2006. Assessment of failure susceptibility of soil slopes using fuzzy logic. Eng. Geol. 86, 211–224.

Torkashvand, A.M., Irani, A., Sorur, J., 2014. The preparation of landslide map by landslide numerical risk factor (LNRF) model and geographic information system (GIS). Egypt. J. Remote Sens. Space Sci. 17, 159–170.

Uzielli, M., Nadim, F., Lacasse, S., Kaynia, A., 2008. A conceptual framework for quantitative estimation of physical vulnerability to landslides. Eng. Geol. 102, 251–256.

Van Westen, C.J., 2013. Remote sensing and GIS for natural hazards assessment and disaster risk management. Ref. Module Earth Syst. Environ. Sci. Treatise Geomorph. 3, 259–298.

Van Westen, C.J., Castellanos, E., Kuriakose, S.L., 2008. Spatial data for landslide susceptibility, hazard, and vulnerability assessment: an overview. Eng. Geol. 102, 112–131.

Vega, J.A., 2013. Risk Estimate by Landslides Generated by Seismic Events in Medellin Using Tools of Geomatics. Application to urban buildings. (In Spanish) (Master Thesis) Faculties of Engineering and Astronomical and Geophysical Sciences, National University of La Plata, Argentina (169 pp.).

Zêrere, J.L., García, R.A., Oliveira, S.C., Reis, E., 2008. Probabilistic landslide risk analysis considering direct costs in the area north of Lisbon (Portugal). Geomorphology 94, 467–495.